Environmental Research 197 (2021) 111133

Contents lists available at ScienceDirect

Environmental Research

journal homepage: www.elsevier.com/locate/envres

Epigenetically modified nucleobases (5hmc, 5fc, and 5caC) interaction with boron and nitrogen doped porous graphene (B/N-pGr) as promising materials for biosensing application: A density functional theory calculations

Vinnarasi Saravanan [a], Akilan Rajamani [a], Shankar Ramasamy [a,*], Alaa Baazeem [b], Indra Raj Upadhyaya [c]

[a] Department of Physics, Bharathiar University, Coimbatore, 641046, Tamil Nadu, India
[b] Department of Biology, College of Science, Taif University, P.O. Box 11099, Taif, 21944, Saudi Arabia
[c] Department of Chemistry Education, Chungbuk National University, Chungcheongbuk-do, 28644, Republic of Korea

ARTICLE INFO

Keywords:
Porous graphene
Modified nucleobases
Bio-sensor
DFT

ABSTRACT

In this present work, porous graphene (pGr), boron (B-pGr), and nitrogen (N-pGr) doped porous sheets are explored as a bio-sensor device for sensing modified nucleobases (MBs) in cancer therapy using density functional theory (DFT). The obtained geometrical, energetic and electronic properties revealed that the B-pGr is highly reactive and it adsorbs MBs better than the pGr and N-pGr, because B atom holds empty p-orbitals which easily interact with partially filled p-orbital of N and O atom. Thus, the adsorption energies of 5hmc, 5caC, and 5fc on B-pGr are high rather than the pGr and N-pGr. The corresponding adsorption energies are −96.074, −77.0, and −60.721 kcal/mol for 5hmc, 5caC, and 5fc respectively. The positive signature of ΔN values (0.005 eV, 0.076 eV, and 0.047 in MBs on pGr and 0.171 eV, 0.252 eV and 0.205 eV in MBs on N-pGr) are obtained at MBs on pGr and N-pGr complex. The negative ΔN values (−0.141 eV, −0.032 eV, and −0.061 eV in MBs on B-pGr) are obtained at MBs of B-pGr. The calculated absorption values shows that the B-pGr is strongly adsorbed MBs at 342 nm. The obtained results exhibit that the B-pGr sheet retains significant therapeutic potential as a bio-sensing application for cancer therapy.

1. Introduction

The expansion of two-dimensional (2D) nanomaterials in nanotechnology received great impact on various fields such as bio-sensor devices, drug delivery application, detect toxic gases for environmental application, and energy harvesting applications. Recently DNA/RNA sensing on 2D nanomaterials received great attention in the pharmacological field to develop personalized medicine for specific diseases. In our previous work, some theoretical prediction has been made to adsorb DNA/RNA base pairs (AT, GC, and AU) on defective and defect-dopant graphene sheet (Saravanan et al., 2020b). These discoveries further lead to adsorb the epigenetic modifications of nucleobases over the graphene-based nanomaterials. The improvement of graphene related nanomaterial depends on our capacity to open a tunable energy gap. Several techniques have been improved to synthesis high-performance graphene-based nanomaterials by engineering their energy gaps to increase their semiconducting properties. Semiconductor based bio-sensor devices are highly challenging because of their exceptional structural stability and surface reactivity in the ambient conditions. The primary challenge of the semiconductor-based bio-sensor devices is to encounter the demand for more sensitivity and specificity. Nowadays, solid-state nanopores (Gershow and Golovchenko, 2007) and biological nanopores (Kasianowicz et al., 1996) are emerging as a powerful technique for next-generation of DNA sequencing method. In recent years, porous graphene (pGr) had a great impact in many fields such as environmental protection, energy storage, energy conversion, water cleaning process, and biomedical applications, due to their semiconducting nature. Typically, porous carbon materials comprise porous or voids with different physical appearance (size and shape) which mainly have exceptional physical and chemical properties such as high mechanical

* Corresponding author.
E-mail address: rshankar@buc.edu.in (S. Ramasamy).

https://doi.org/10.1016/j.envres.2021.111133
Received 9 March 2021; Received in revised form 31 March 2021; Accepted 1 April 2021
Available online 18 April 2021

strength, high sensitivity, and good electrical and thermal conductivity. Predominantly, the porous carbon material is an outstanding material with a low density and high specific strength (Wasalathilake and Ayoko, n.d.). It is also capable of bonding with neighbour atoms through its sp, sp^2, and sp^3 hybridization. The high sensing mechanism is a very smart application for porous graphene due to the high surface area and additional porosity, which could lead to better bio-sensing applications. Hence, in this work, pGr is used as a template material to adsorb epigenetically modified nucleobases (MBs) for cancer therapy. Previous studies reported that the presence of dopant atom increases the chemical reactivity of 2D nanomaterials surface. The dopant atom such as boron (B), nitrogen (N), silicon (Si), aluminium (Al), and phosphorous (P) atoms enhance the chemical reactivity of the graphene surface (Ao et al., 2010; Dai et al., 2009; Mudedla et al., 2014). Previous findings (Agnoli and Favaro, 2016) have reported that B dopant atom modifies the physical and chemical properties of graphene nanomaterials, thus, it could be used for biomolecular detection and separation technology applications. Therefore, in this exploration pGr, B, and N doped pGr are used as a bio-sensor device to adsorb MBs using the theoretical approach.

Canonical epigenetic modifications, comprising nucleic acid methylation, histone alteration, and chromatin remodelling, play an essential role in several life progression mainly neurodevelopment and other human diseases (Meng et al., 2019). Epigenetic modification elucidates the growth of cells in an organism with the same DNA sequence into diverse cell types with numerous functions. For the past few years, several studies revealed that the appearance of abnormal epigenetic modifications in DNA always related with the occurrence of several diseases, comprising cancer, diabetes, Alzheimer and many age-related diseases (Dolinoy et al., 2007; Hatchwell and Greally, 2007; Petronis, 2010; Portela and Esteller, 2010). DNA modification was mostly used in initial stages to refer 5-methylcytosine (5-mc), which acts as an important characteristic in many biological processes such as gene expression in regular cell development, X-chromosome inactivation, and maintenance of genome stability (Ito et al., 2011; Lu et al., 2015; Schübeler, 2015). In mammal cells, cytosine methylation is generally intermediated by the ten-eleven translocation methyl-cytosine dioxygenase (TET) family. TET protein belongs to the family of iron (II)/alpha-ketoglutaric acid dependent dioxygenases (Lu et al., 2015), which are primarily found to oxidize 5-mc to 5-hydroxymethylcytosine (5-hmc). Later findings have reported that 5-hmc can be further oxidized by TET protein to generate 5-formylcytosine (5-fc) and 5-carboxylcytosine (5-caC) (Cheng et al., 2015; Hahn et al., 2014; Ito et al., 2011). The epigenetically modified 5-fc and 5-caC are selectively distinguished and detached by thymine DNA glycosylase (TDG), and repaired to normal cytosine through base excision repair (Bian et al., 2019; He et al., 2011; Xing et al., 2018). 5-fc and 5-caC are less plentiful than 5-hmc and it can be a stable epigenetic mark that regulates transcription process (Hahn et al., 2014; Xing et al., 2018; Xu et al., 2014). In specific, 5hmc distributes throughout the genome and it appears to act a dynamic role in the central nervous system, where it exists in higher level compared with embryonic stem cells and other normal cells (Szwagierczak et al., 2010). Hence, in this investigation, an attempt has been made to scrutinize the adsorption mechanism of 5hmc, 5fc, and 5caC (denoted as MBs) over the porous graphene derivatives (pGr, B-pGr, and N-pGr (denoted as p-GDs)) by DFT. The following key points have been addressed in this present investigation. i) The geometrical, electronic and global reactivity parameters are calculated for pGr and its doped porous model (B-pGr and N-pGr) to understand the adsorption capacity and structural reactivity. ii) To govern the adsorption strength of MBs on p-GDs and compare adsorption strength of MBs on pGr and its doped porous model (B-pGr and N-pGr). iii) The charge transfer direction and orbital interactions are carried out for MBs on pGDs during complexation. iv) To assess the interactive nature between MBs and p-GDs. v) The absorption properties are investigated upon MBs adsorption on p-GDs.

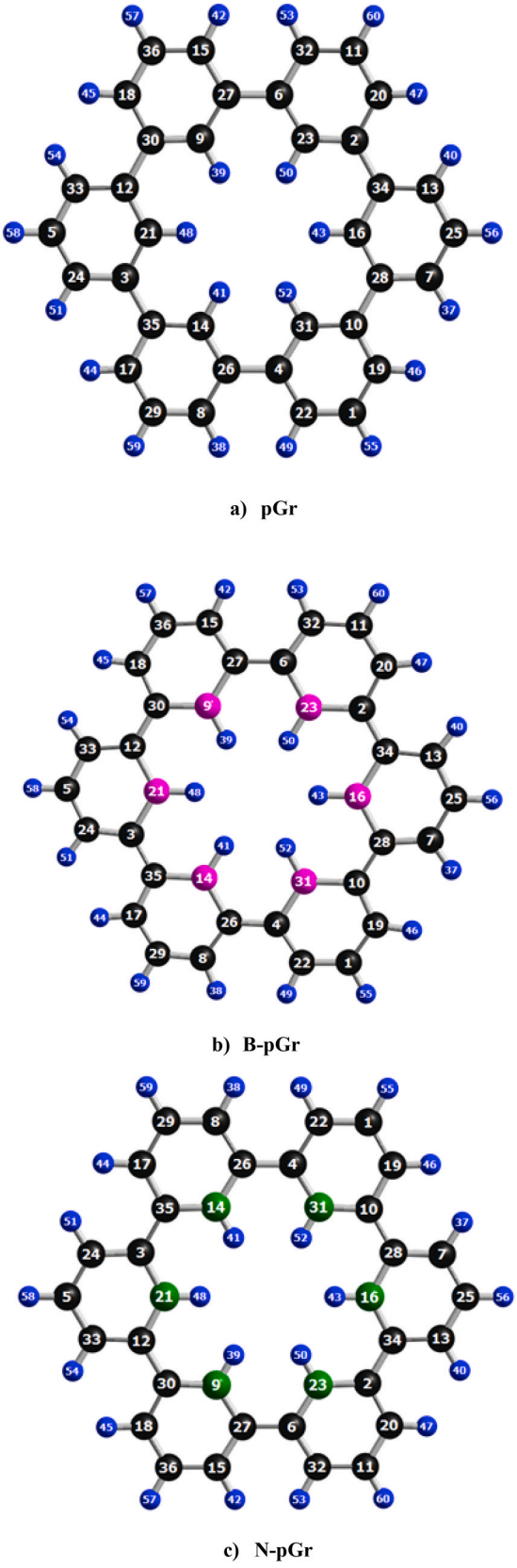

a) pGr

b) B-pGr

c) N-pGr

Fig. 1. The optimized structure of p-GDs. Here black color is C, pink is B, green is N, and blue is H. (For interpretation of the references to colour in this figure legend, the reader is referred to the Web version of this article.)

Table 1
The structural properties of 5hmc, 5fc, and 5caC calculated by M06–2X/6–31 + g* level of theory.

Bond type	5 hmc (Å)	5fc (Å)	5caC (Å)
C=O	1.222 (1.23)*[a]	1.223 (1.24)*[a]	1.216 (1.20)*[b]
C–C	1.411 (1.45)*[a]	1.456 (1.46)*[a]	1.458 (1.45)*[b]
C=N	1.319 (1.32)*[a]	1.310 (1.33)*[a]	1.309 (1.40)*[b]
N–H	1.015	1.015	1.015
C–H	1.092	1.089	1.088

*a Ref (Mato et al., 2017) and.
*b Ref (Xing et al., 2018).

Table 2
The structural properties of pGr, B-pGr, and N-pGr calculated by M06–2X/6–31 + g* level of theory.

Bond type	pGr (Å)	B-pGr (Å)	N-pGr (Å)
C – C	1.499 (1.46)*[a]	1.451	1.428
C = C	1.407	1.406	1.396
C – H	1.084	1.089	1.080
B – C	–	1.568 (1.50*[a], 1.497*[c])	–
B – H	–	1.167 (1.19)*[b]	–
N – C	–	–	1.424 (1.37)*[a]
N – H	–	–	1.003

*a Ref (Li et al., 2015).
*b Ref (Wang et al., 2019), and *[c] Ref (Kong et al., 2012).

2. Computational methodology

The current investigation explores the adsorption mechanism of MBs on p-GDs by the M06–2X (Zhao and Truhlar, 2008) and wB97XD (Salzner and Aydin, 2011) functional with 6–31 + g* level of theories using the Gaussian 09 program (Frisch et al. (2009)). The M06–2X basis functional is the highly parameterized approximate exchange-energy correlation function and it is indirectly deal with "medium range (≤5 Å)" electron correlation, and not for long range interaction (>5 Å). Here, we have selected another functional wB97XD to describe the long-range correction (i.e. stacking interaction). The isolated 5-hmc, 5fc, 5caC, pGr, B-pGr, and N-pGr optimized by the above level theories and their structural stability is verified by the frequency analysis. The inter-molecular complexes of MBs with p-GDs optimized by the M06–2X/6-31 + G* level of theory. The adsorption energy is calculated by the counterpoise (CP) method (Taylor et al. n.d.) with basis set superposition error correction (BSSE) employing M06–2X and wB97XD level of theories. The calculated adsorption energy equation is given below

$$E_{ads} = E_{MBs+p\text{-}GDs}\text{-}(E_{MBs} + E_{p\text{-}GDs}) \quad (1)$$

Here, $E_{MBs+p\text{-}GDs}$ are total adsorption energy of MBs on p-GDs, E_{MBs}, and $E_{p\text{-}GDs}$ individual energy of monomers respectively. The structural stability, chemical reactivity, and adsorption capability are calculated by global reactivity descriptors for p-Gr and doped porous doped model. The charge transfer direction is also investigated for MBs on p-GDs by following equations,

$$\Delta N = \frac{(\mu_B - \mu_A)}{\eta_A + \eta_B} \quad (2)$$

where, μ_A, μ_B, η_A and η_B are chemical potential and hardness of acceptor and donor region. Here A is an acceptor (MBs) and B is a donor region (p-GDs). If ΔN parameters have a positive signature, the charge will be transferred from p-GDs to MBs or it is in reverse direction (Saravanan et al., 2020a). Further, corresponding orbital interactions are calculated for MBs on p-GDs by natural bond order (NBO) analysis (Reed et al., 1988). In the present investigation, atoms in molecule (AIM) analysis is used to predict both covalent and non-covalent interaction during complexation using bond critical points (BCPs) (Bader, 1991a) by Multiwfn (Lu and Chen, 2012) source code. The sensitivity of p-GDs towards adsorption of MBs are assessed by the density of state (DOS) analysis (Saravanan et al., 2020c). The optical property is explored for MBs on P-GDs by the time-dependent density functional theory (TD-DFT).

3. Results and discussion

3.1. Structural properties of monomers

The pGr holds 36 carbon (C) atoms and 24 hydrogen (H) atoms passivate at the edge and porous region of the sheet. Zhang et al. (2013) suggested that the edge passivation is alternative way to decrease the effect of edge stresses for graphene sheet. In this current exploration, six boron (B) and six nitrogen (N) substitutes the C atom at C_9, C_{14}, C_{16}, C_{21}, C_{23}, and C_{31} positions. The atomic masses of B and N substituents are closest to C atom, which would be suitable as carbon substitute, whereas the substitution considerably modifying the electronic properties of the host material due to the electron-rich and electron-deficient nature of N and B atoms. The optimized geometry of p-GDs structures is given in Fig. 1.

The isolated 5hmc, 5fc, and 5caC modified nucleobases are optimized by the M06–2X level of theory and their structural properties are given in Table 1 and optimized structures are shown in Fig. 2, these results are good agreement with previous reported results (Mato et al., 2017; Xing et al., 2018).

In p-Gr, the calculated bond length of C – C, C═C, and C–H are 1.499 Å, 1.407 Å, and 1.084 Å respectively and these results are close agreement with previous results (AlZahrani and Srivastava, 2010; Liu et al., 2013; Pashangpour and Ghaffari, 2013; Sofo et al., 2007), the

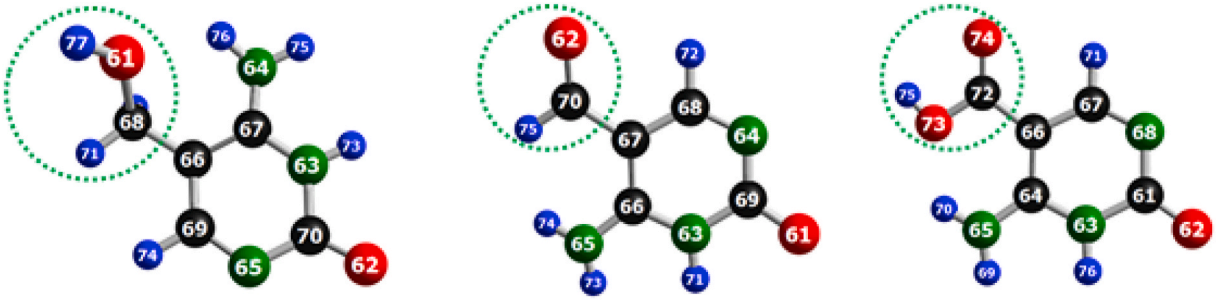

Fig. 2. The optimized structure of epigenetically modified bases. Here black color is C, red is O, green is N, and blue is H. (For interpretation of the references to colour in this figure legend, the reader is referred to the Web version of this article.)

Table 3
The global reactivity parameters are calculated for pGr, B-pGr, and N-pGr by M06–2X/6–31 + g* level of theory.

p-GDs	Energy gap (eV)	μ (eV)	η (eV)
pGr	4.130 (3.7, 3.2)*[a]	3.88	2.07
B-pGr	1.280	4.72	0.64
N-pGr	1.224	2.76	0.61

*a Ref (Xu et al., 2012).

corresponding values are given in Table 2.

While B doping, the C – C, C═C and C – H bond lengths are found to be 1.480 Å, 1.407 Å, and 1.089 Å respectively. Compared with p-Gr, C – C, C═C and C – H bond lengths are slightly elongated in B-pGr case due to large atomic radius of B atom. Whereas, in the case of N-pGr, the calculated bond lengths of C – C, C═C and C – H are 1.427 Å, 1.396 Å, and 1.085 Å respectively. Compared with p-Gr and B-pGr, N-pGr bond lengths are contracted which is mainly due to the smaller atomic radius N atom present in the porous region, these results are consistent with the previous result (Saravanan et al., 2020b). The B – C and N – C calculated bond lengths values are 1.502 Å and 1.424 Å, these results are well correlated with previous results (1.497 Å and 1.412 Å) (Andriotis et al., 2016; Hu et al., 2020; Kong et al., 2012; Shukla et al., 2017; Singh et al., 2017). Compared to B–C bond, N–C bond has smaller bond length, because N (3.04) has higher electronegativity which makes a stronger bond with C atom (Saravanan et al., 2020b), which is also verified by electron density (ρ(r)) value. The calculated ρ(r) values of B – C and C – N are found to be 0.181 and 0.277 a.u. The B and N dopant atoms increase the charge transfer from −0.208 e to −0.324 e and −0.271 e, these results are good agreement with previous result [38,39] within the B-pGr and N-pGr. Increasing charge transfer further reduces the energy gap between the highest occupied molecular orbital (HOMO) to the lowest unoccupied molecular orbital (LUMO). The energy gap between the HOMO and LUMO values of p-Gr is decreased from 4.130 eV, to

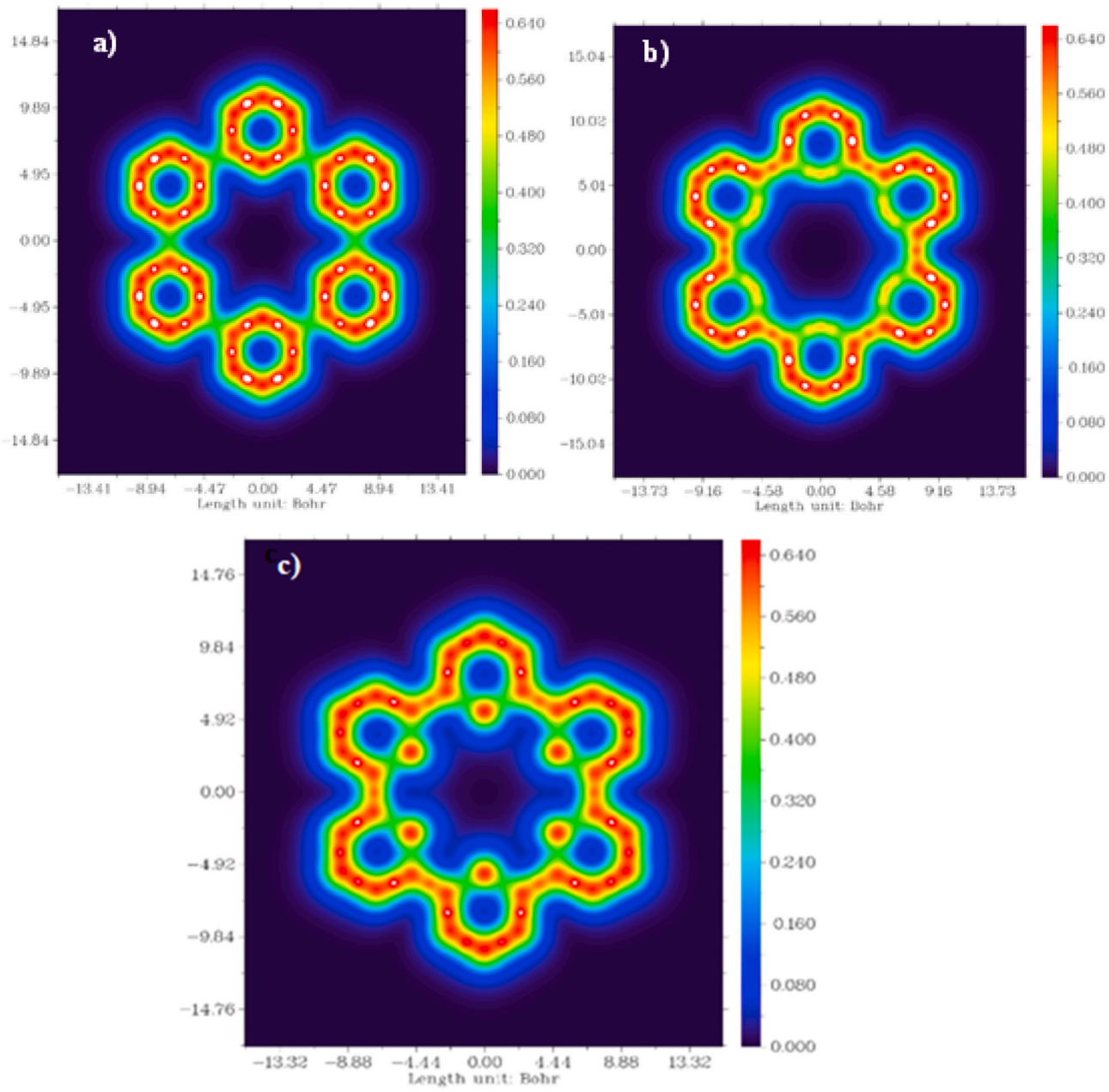

Fig. 3. The electron localized function map of a) pGr, b) B-pGr, and c) N-pGr.

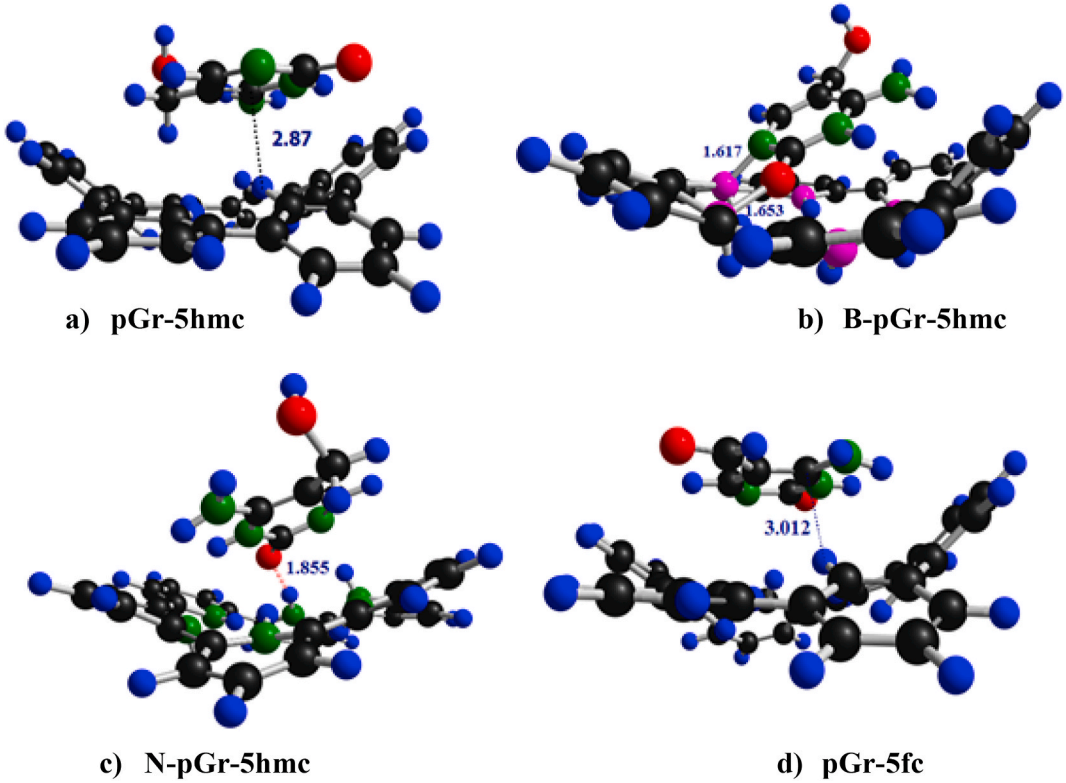

Fig. 4. The optimized structure of MBs on pGDs complex system.

1.280 eV in B-pGr, and 1.224 eV in N-pGr, which are given in Table 3.

The smaller energy gap value of B-pGr and N-pGr surface has high chemical reactivity and it adsorb MBs more than the P-Gr which is further confirmed by global reactivity parameters such as such chemical potential (μ) and hardness (η). The calculated μ and η values are found to be 3.88 eV & 2.07 eV in pGr, 4.72 eV & 0.64 eV in B-pGr, and 2.76 eV & 0.61 eV in N-pGr. The maximum η and minimum μ values expose that the structure is more stable and less reactive nature (Saha and Bhattacharyya, 2016). Here, pGr has higher η value than B-pGr and N-pGr which clearly shows that the B-pGr and N-pGr are more reactive and less stability. Moreover, the structure aromaticity is calculated for pGr, B-pGr, and N-pGr using PDI (Matito et al., 2006). The calculated PDI value of pGr, B-pGr, and N-pGr are 0.092, 0.045, and 0.044 respectively. The pGr possess larger aromaticity value than the others, due to the π-electrons, which are highly delocalized within the benzene ring and it is stronger than B-pGr and N-pGr (Matito et al., 2006). This result is in good agreement with electron localized function (ELF) which is given in Fig. 3. In ELF, red and blue colours represent electron depletion and high electron concentration region. In Fig. 3, the π-electrons are highly delocalized within the p-Gr system compared to B-pGr, and N-pGr. A major inadequacy of p-Gr surface is chemically inert because of the strong sp^2 hybridization and delocalized electron between C–C atoms in the p-Gr surface, hence, the interaction between the p-Gr and the MBs are fairly weak than the B-pGr and N-pGr. The geometrical properties conclude that B-pGr and N-pGr adsorb MBs more than p-Gr.

3.2. Structural properties of MBs on p-GDs

The MBs bases are placed parallel ($\pi - \pi$ stacking) to the basal plane of the p-GDs at 3 Å distances. After complex formation, the $\pi - \pi$ stacking distance between MBs and p-GDs are decreased as shown in Fig. 4.

The calculated stacking distance of MBs on p-Gr, B-pGr, and N-pGr complex are 2.6–2.8 Å, 1.5–1.6 Å, and 1.9–2.6 Å respectively. Among complexes, the p-Gr is slightly adsorbing MBs on it, due to their chemically inert surface. The B-pGr covalently interacts with MBs bases because, during complex formation, the high charge (−0.33 e) is relocated from high electronegative (N/O) atom to electropositive (B) atom. The B atom holds empty p-orbitals which easily interact with partially filled p-orbital of N and O atom (Berski et al., 2011), thus, it is covalent bond interaction during the complexation process, which confirmed by QTAIM analysis. The calculated B–O and B–N bond lengths of MBs-B-pGr complexes are found to be 1.653 Å and 1.616 Å in 5hmc, 1.585 Å in 5fc, and 1.544 Å in 5caC. The corresponding electron density values are found 0.079 a.u & 0.114 a.u in B-pGr-5hmc, 0.097 a.u in B-pGr-5fc, and 0.109 a.u in B-pGr-5caC. In case of MBs-N-pGr complex the H-bond interactions are obtained between O/N atom in MBs and H atom in N-pGr, due to H-bond interaction, the stacking distance between MBs and N-pGr is reduced from 3 Å to 1.9–2.6 Å. Due to covalent and H-bond interactions, the adsorption energies are higher for B-pGr and N-pGr with 5hmc, 5fc, and 5caC bases than pGr-complex. The obtained geometrical properties show that the B-pGr is more reactive and it adsorbs more MBs on it.

3.3. Adsorption energy

The adsorption energy is an important technique to understand the total adsorption energy between two or more species. The total adsorption energy is calculated for the MBs on p-GDs with the assist of counterpoise with BSSE correction by the M06–2X level of theory. The calculated total adsorption energy values of complexes are given in Table 4.

Tabatabaei et al. (2018), have been found that the total adsorption energies of 5hmc, 5fc, and 5caC on the MoS_2 sheet are −0.68 eV, −0.52 eV, and −0.63 eV respectively. Lately, Gao, H et al. (Gao et al., 2019), have been reported that graphene nanoflake adsorbs MBs more than

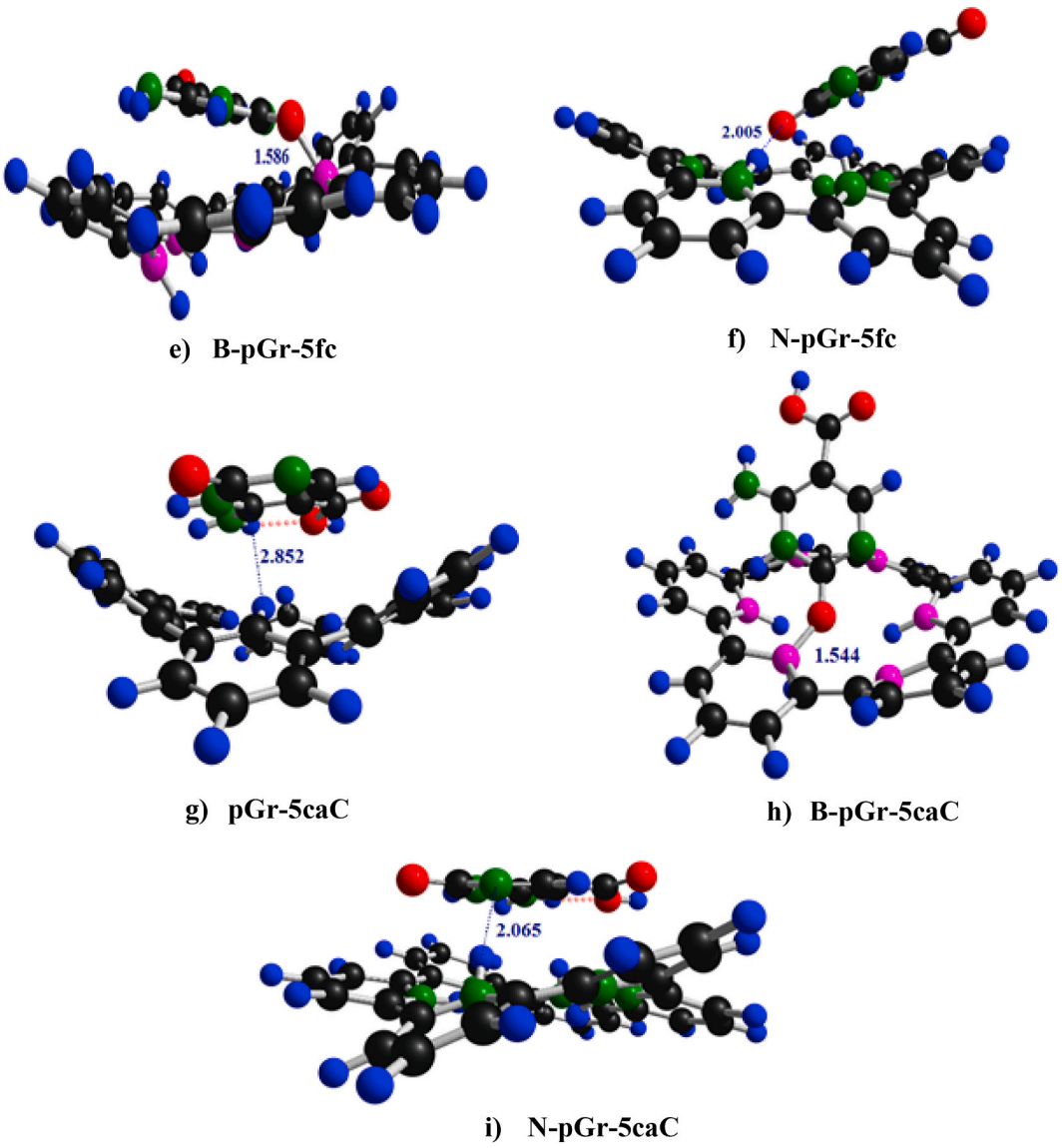

Fig. 4. (*continued*).

Table 4
The adsorption energy and charge transfer values of complex system.

Complex system	Adsorption Energy (kcal/mol)		Charge transfer value
	M06–2X in	wB97XD in	ΔN in eV
pGr-5hmc	−16.573	−17.595	0.005
B-pGr-5hmc	−94.614	−96.074	−0.141
N-pGr-5hmc	−35.350	−36.274	0.171
pGr-5fc	−15.215	−19.316	0.076
B-pGr-5fc	−84.761	−60.721	−0.032
N- pGr-5fc	−23.830	−38.943	0.252
pGr-5caC	−19.157	−21.003	0.047
B-pGr-5caC	−68.745	−77.0	−0.061
N-pGr-5caC	−22.975	−24.062	0.205

normal DNA base i.e. cytosine base, which is mainly due to the hydroxyl, formyl, and hydroxyl functional group present at the MBs which enhance the adsorption energy. Their total adsorption energy of cytosine, 5fc, 5hmc, and 5caC with graphene nanoflake are −15.15 kcal/mol, −17.13 kcal/mol, −17.83 kcal/mol, and −16.18 kcal/mol. Tabatabaei et al. (2018) and Gao, H et al. (Gao et al., 2019) also reported that 5hmc and 5caC are adsorbed more on MoS_2 and graphene nanoflake than 5fc base. In this present exploration, the total adsorption energies are calculated by the M06–2X/6–31 + g* level of theory. The calculated total adsorption energy values of MBs on pGr are −16.573 kcal/mol (5hmc), −15.215 kcal/mol (5fc), and −19.157 kcal/mol respectively. When B and N atom doped at the porous site, the surface sensitivity and selectivity also increase, thus, they highly adsorb MBs than pGr. The calculated total adsorption energy values of MBs on B-pGr are −94.614 kcal/mol (5hmc), −84.761 kcal/mol (5fc), and −68.745 kcal/mol (5caC) respectively. In the case of MBs on N-pGr, the total adsorption energy values are found to be −35.350 kcal/mol (5hmc), −23.830 kcal/mol (5fc), and −22.975 kcal/mol (5caC) respectively. Among all complex systems, MBs with B-pGr has higher total adsorption energy due to the covalent bond formation during complexation. At long-range interaction (>5 Å), the hybrid M06–2X functional is incapable to appropriately explain the R-6 asymptotic distance-dependence of dispersion forces (Langreth et al., 2005). Therefore, hybrid DFT functional with long-range corrections is very vital to define the stacking interaction between two different monomers. The wB97XD functional incorporates the long-range correction (LC) with empirical atom-atom dispersion corrections (DFT-D) and it also explicit the empirical dispersion correction term R-6 (Chai and Head-Gordon, 2008; Kamel et al., 2017). Hence, the effect of dispersion method has also been

Table 5
The charge transfer mechanism is calculated by NBO analysis.

Complex System	Donor	Acceptor	$E^{(2)}$ kcal/mol
pGr-5hmc	π C_7–C_{25}	σ^*N_{63}–H_{73}	1.55
	π C_4–C_{31}	σ^*O_{62}–C_{70}	1.64
	LP N_{64}	σ^*C_{23}–H_{50}	0.58
	σ^*N_{65}.C_{69}	π^*C_{14}–C_{26}	1.47
B-pGr-5hmc	σ B_{23}–H_{50}	σ^*B_{23}–N_{65}	27.86
	σ B_{23}–N_{65}	LP* C_{70}	152.65
	σ B_{23}–N_{65}	π^*C_{66}–C_{69}	57.09
	σ O_{62}–C_{70}	LP* B_9	22.82
	σ N_{65}–C_{69}	σ^*B_{23}–N_{65}	24.30
	σ N_{65}–C_{70}	σ^*B_{23}–N_{65}	23.07
N-pGr-5hmc	π C_3–C_{24}	σ^*N_{64}–H_{75}	2.99
	σ O_{62}–C_{70}	σ^*N_{23}–H_{50}	2.07
	σ N_{23}–H_{50}	LP* O_{62}	11.25
	LP N_{63}	σ^*N_{14}–H_{41}	1.21
	σ^*N_{16}–H_{43}	LP N_{65}	4.79
	π^*C_{66}–C_{67}	π^*C_4–C_{26}	1.09
pGr-5fc	π^*C_9–C_{27}	π^*O_{61}–C_{69}	1.68
B-pGr-5fc	π^*O_{61}–C_{69}	LP* B_9	29.17
	LP O_{61}	LP* B_9	100.94
	LP O_{61}	σ^*B_9–C_{27}	4.17
N- pGr-5fc	π C_3–C_{35}	π^*C_{66}–C_{67}	1.11
	π C_5–C_{24}	σ^*N_{65}–H_{73}	1.58
	π C_{12}–C_{33}	σ^*N_{63}–H_{71}	1.86
	LP N_{14}	π^*O_{61}–C_{69}	1.80
	σ N_{64}–C_{68}	σ^*N_{31}–H_{52}	1.52
	σ N_9–H_{39}	LP* O_{61}	6.70
	LP O_{61}	σ^*N_{16}–H_{43}	3.82
	σ N_{31}–H_{52}	LP* O_{64}	9.41
pGr-5caC	π C_{14}–C_{26}	π^*C_{72}–O_{74}	3.12
B-pGr-5caC	LP C_{34}	σ^*N_{63}–H_{76}	13.31
	π C_{61}–O_{62}	LP* B_{23}	33.27
	LP O_{62}	LP* B_9	12.87
	LP O_{62}	LP* B_{23}	12.50
	LP O_{62}	σ^*C_2–B_{23}	4.73
	LP O_{62}	LP* B_{23}	138.31
	LP O_{62}	σ^*B_{23}–H_{50}	3.19
N-pGr-5caC	π C_3–C_{24}	σ^*N_{65}–H_{69}	2.13
	LP N_{16}	σ^*C_{67}–N_{68}	1.04
	σ C_{67}–N_{68}	σ^*N_{23}–H_{50}	3.08
	σ N_{23}–H_{50}	LP* N_{68}	8.37

computed for the MBs on p-GDs. In this present investigation, the total adsorption energy values of all complex system are calculated by the wB97XD/6–31 + g*. The calculated total adsorption energy values of 5hmc on pGr, B-pGr, and N-pGr are −17.595 kcal/mol, −96.074 kcal/mol, and −36.274 kcal/mol respectively. In 5fc over pGr, B-pGr, and N-pGr, the adsorption values are −19.316 kcal/mol, −60.721 kcal/mol, and −38.943 kcal/mol respectively. Similarly, in the case of 5caC over pGr, B-pGr, and N-pGr, the calculated adsorption values are −21.003 kcal/mol, −77.0 kcal/mol, and −24.062 kcal/mol respectively. The adsorption energy order of MBs on p-GDs is B-pGr-5hmc > B-pGr-5caC > B-pGr-5fc > N-pGr-5fc > N-pGr-5hmc > N-pGr-5caC > pGr-5caC > pGr-5fc > pGr-5hmc. The overall adsorption energy results clearly display that B-pGr has more adsorption energy for 5hmc, 5fc, and 5caC than the N-pGr and pGr. The orders of the reactive sheets are B-pGr > N-pGr > pGr. The highest adsorption is due to the strongest interaction arises between B (in B-pGr) and O/N (in 5hmc, 5fc, and 5caC bases). Among MBs on p-GDs complex, 5hmc is more adsorb with B-pGr (−96.074 kcal/mol) than the other two MBs, because two covalent bond interactions arise during complexation process (N_{65}–B_{23} and O_{62}–B_9) between 5hmc and B-pGr. Compared with pGr, N-pGr is adsorbed more 5hmc, 5fc, and 5caC bases, due to their small energy gap value and chemical hardness. The total adsorption energy result shows that B-pGr would be a good sensing device and it would be potentially efficient in cancer therapy. Moreover, B-pGr is more appropriate for 5hmc base when compared to 5fc and 5caC bases.

3.4. Charge transfer characteristics

The charge transfer mechanism is playing an important role to understand the amount of charge transfer between intra and intermolecular complex of two systems. In this work, the charge transfer characteristic is computed for MBs on the p-GDs by natural bond order NBO and electron density difference map (EDDM) analysis. Moreover, the electron transfer direction is investigated for all complex system by ΔN parameter values and these values are compared with NBO analysis (Vatanparast and Shariatinia, 2018). The calculated stabilization energy (E^2) values of complexes are given in Table 5.

According to Table 5, the most substantial proton-donor and proton-acceptor in the 5 hmc-pGr are πC_7–$C_{25} \rightarrow \sigma^*N_{63}$–$H_{73}$ and πC_4–$C_{31} \rightarrow \sigma^*O_{62}$–$C_{70}$, their corresponding E^2 values are 1.55 kcal/mol and 1.64 kcal/mol. In 5 hmc-pGr complex, pGr (π C_7–C_{25} and π C_4–C_{31}) is a proton donor and 5hmc (σ^*N_{63}–H_{73} σ^* O_{62}–C_{70}) is a proton acceptor region, which reveals that the existence of π-π stacking interaction and it occurs between 5hmc and pGr. The highest charge is transferred between π^*O_{61}–C_{69} (donor) and π^* C_9–C_{27} (acceptor), their corresponding E^2 value is 1.68 kcal/mol in 5fc-pGr complex. In the case of pGr-5caC complex, πC_{14}–C_{26} (pGr) is a donor region and π^*C_{72}–O_{74} (5caC) is an acceptor, their calculated E^2 value is 3.12 kcal/mol. When compared with 5hmc and 5fc, 5caC on pGr has the highest E^2 value, due to the highest charge (0.33 e) is transferred between pGr and carboxyl group of 5caC during complex formation. Thus, pGr-5caC complex has higher adsorption energy than the pGr-5fc and pGr-5hmc. This result confirms that the functional group enhances the adsorption energy between MBs and pGr (Gao et al., 2019). The charge transfer order is pGr-5caC > pGr-5fc > pGr-5hmc; this result is well correlated with adsorption energy analysis. The NBO results strongly report that the charge is transferred from pGr to MBs during complex formation which is further verified by ΔN parameter. The positive value of ΔN signifies that the electron transfer is occurred from pGr to MBs, the negative signature of ΔN shows vice versa. The ΔN parameter values of 5hmc, 5fc, and 5caC on pGr are 0.005 eV, 0.076 eV, and 0.047 eV respectively, which are given in Table 4. The positive ΔN value defines that pGr is a donor region and MBs is an acceptor region. In MBs with B-pGr complexes, the highest charge transfer has occurred from σB_{23}-N_{65} to LP*C_{70} in B-pGr-5hmc, LPO_{61} to LP*B_9 in B-pGr-5fc, and LP O_{62} to LP* B_{23} in B-pGr-5caC. The corresponding E^2 values are 152.65 kcal/mol, 100.94 kcal/mol, and 138.31 kcal/mol respectively. The highest E^2 value is mainly due to the strong covalent bond interaction between B and O/N atoms. During complexation process, the high amount of charge (0.358 e) is relocated from high electronegative atom (O/N) to electropositive atom (B), thus it gets higher adsorption energy than the other complex systems. The order of E^2 is B-pGr-5hmc > B-pGr-5caC > B-pGr-5fc, this result is well correlated with adsorption energy analysis. These results show that the charge is transferred from MBs to B-pGr; this is further confirmed by the ΔN parameter values. The ΔN values of MBs with B-pGr are −0.141 eV, −0.032 eV, and −0.061 eV. Here, the negative signature of ΔN values indicates that the electron flow is relocated from MBs to B-pGr. In MBs on N-pGr complex, the hydrogen bond interactions are observed in 5hmc and 5fc with N-pGr. In N-pGr-5hmc, N_{23}–$H_{50}\cdots O_{62}$ and N_{16}–$H_{43}\cdots N_{65}$ hydrogen bonds are observed, their corresponding E^2 values are 11.25 kcal/mol and 4.79 kcal/mol. Here in the N-pGr-5hmc complex, σN_{23}–H_{50} and σN_{16}–H_{43} are proton-donor, whereas, LP* O_{62} and LP* N_{65} are proton-acceptor regions. Correspondingly, in N-pGr-5fc and N-pGr-5caC complex, σN_9–H_{39}, σN_{31}–H_{52}, and σ N_{23}–H_{50} are proton-donor region, whereas, LP* O_{61}, LP* O_{64}, and LP* N_{68} are proton-acceptor region. The corresponding E^2 values are 6.70 kcal/mol, 9.41 kcal/mol, and 8.37 kcal/mol. The calculated ΔN values of MBs with

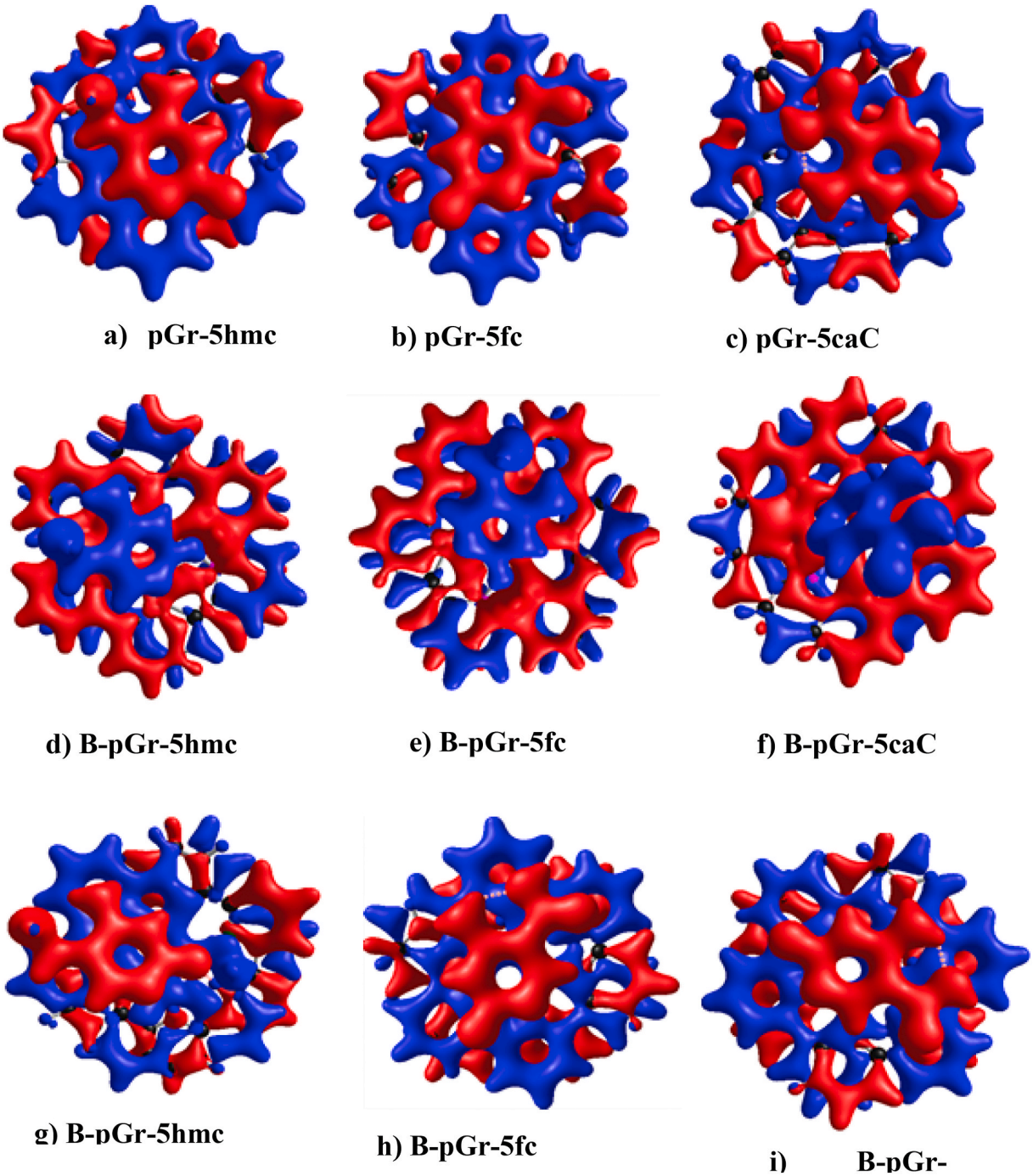

Fig. 5. Electron density difference map of MBs on pGr, B-pGr, and N-pGr complex system.

N-pGr are 0.171 eV in N-pGr-5hmc, 0.252 eV in N-pGr-5fc, and 0.205 eV in N-pGr-5caC. The NBO analysis and positive value of ΔN report that the charge transfer occurs from N-pGr to MBs in complex formation. The charge transfer mechanism is further verified by the EDDM analysis which is shown in Fig. 5. The red and blue colours represent the concentration of electron increases (rich region) and decrease (depletion region) region respectively, which are given in Fig. 5. In pGr-MBs and N-pGr-MBs complexes, the electron-rich region is scattered on MBs and electron depletion region is fell on pGr and N-pGr, which means the charge is transferred from pGr and N-pGr to MBs. In contrast, the charge transfer has occurred from MBs to B-pGr in B-pGr-MBs complex which is mainly due to the strong covalent interactions appearing between B and N/O in B-pGr-MBs complex. Thus, the B-pGr-MBs complexes have higher adsorption energy than the other complex system.

3.5. Topological properties

Atoms in molecule (AIM) analysis is used to comprehend the interaction nature (either covalent or non-covalent) and bonding strength between two atoms in a molecular system (Bader, 1991b). Hence, in this exploration, AIM is used to examine the interaction between MBs and p-GDs. The electron density ρ(r), Laplacian electron density $\nabla^2\rho$ (r), and total electron density H(r) at the bond critical points (BCPs) are very useful to designate the strength of bond and their interaction (Parthasarathi et al., 2006). The positive and negative H(r) value specifies the non-covalent and covalent interaction between two systems. Further,

Table 6
Topological parameter values of isolated and complex system are calculated by QTAIM.

Complex System	Bonding type	ρ(r) in a.u	$\nabla^2\rho$(r) in a.u	H(r) in a.u	-G(r)/V(r) in a.u
pGr	C–C	0.259	−0.625	−0.216	0.216
	C=C	0.305	−0.814	−0.299	0.241
	C–H	0.279	−0.982	−0.281	0.114
B-pGr	C–C	0.280	−0.699	−0.252	0.235
	C=C	0.396	−0.817	−0.300	0.242
	C–H	0.276	−0.953	−0.274	0.115
	B–C	0.181	−0.694	−0.181	0.475
	B–H	0.194	−0.397	−0.214	0.349
N-pGr	C–C	0.293	−0.752	−0.275	0.240
	C=C	0.310	−0.842	−0.312	0.245
	C–H	0.281	−0.997	−0.286	0.113
	N–C	0.277	0.784	−0.387	0.331
	N–H	0.338	−0.017	−0.471	0.099
pGr-5hmc	H_{71}–C_{24}	0.006	0.017	0.0009	1.380
	H_{72}–C_{21}	0.007	0.025	0.0010	1.102
	N_{65}–C_4	0.006	0.021	0.0008	1.292
	O_{62}–C_{31}	0.010	0.030	0.0008	1.304
B-pGr-5hmc	O_{62}–B_9	0.079	0.443	−0.035	0.807
	N_{65}–B_{23}	0.114	0.449	−0.071	0.720
N-pGr-5hmc	O_{62}–H_{50}	0.030	0.106	0.00003	0.991
	O_{62}–N_9	0.012	0.045	0.0011	1.224
	N_{21}–H_{73}	0.009	0.032	0.0010	1.166
	O_{61}–H_{76}	0.018	0.063	0.0002	1.015
pGr-5fc	O_{61}–C_6	0.005	0.015	0.0006	1.227
	N_{64}–H_{39}	0.007	0.026	0.0012	1.289
	O_{62}–C_{35}	0.005	0.017	0.0007	1.160
	N_{63}–C_{23}	0.006	0.017	0.0005	1.120
B-pGr-5fc	O_{61}–B_9	0.097	0.538	−0.0450	0.799
	N_{64}–B_{21}	0.007	0.022	0.0012	1.343
	N_{63}–B_{23}	0.008	0.021	0.0004	1.080
N- pGr-5fc	O_{61}–N_{21}	0.005	0.016	0.0004	1.124
	O_{61}–H_{39}	0.023	0.074	−0.0006	0.969
	O_{61}–N_{23}	0.009	0.030	0.0005	1.078
	O_{61}–H_{43}	0.022	0.052	−0.00006	0.995
pGr-5caC	O_{74}–C_3	0.006	0.019	0.0007	1.221
	O_{74}–C_{35}	0.006	0.018	0.0007	1.202
	O_{73}–C_{14}	0.006	0.019	0.0006	1.162
	N_{65}–C_{16}	0.007	0.019	0.0006	1.189
B-pGr-5caC	O_{62}–B_{23}	0.109	0.618	−0.0510	0.800
	O_{62}–H_{43}	0.008	0.030	0.0012	1.234
	O_{62}–C_{27}	0.017	0.059	0.0010	1.079
N-pGr-5caC	O_{62}–N_9	0.008	0.025	0.0005	1.086
	N_{68}–H_{50}	0.020	0.062	0.0002	0.943

covalent and non-covalent interaction is verified by the ration of -G(r)/V(r). The -G(r)/V(r)≥1 is non-covalent and -G(r)/V(r) ≤ 1 is a covalent nature (Bader, 1998; Louit et al., 2003). The ρ(r))≥ 0.1 value is covalent, whereas the ρ(r)≤0.01 indicates the non-covalent interaction (Mudedla et al., 2016). The calculated parameter values are given in Table 6.

According to Table 6, the calculated ρ(r) value ranges are 0.006–0.010 a.u in pGr-5hmc, 0.005–0.007 a.u in pGr-5fc, and 0.006–0.007 a.u in pGr-5caC. Their corresponding $\nabla^2\rho$(r) values are 0.017–0.030 a.u in pGr-5hmc, 0.015–0.026 a.u in pGr-5fc, and 0.018–0.019 a.u in in pGr-5caC. The calculated H(r) and –G(r)/V(r) values are 0.0008–0.0010 a.u & 1.102–1.380 a.u in pGr-5hmc, 0.0005–0.0012 a.u & 1.160–1.289 a.u in pGr-5fc, and 0.0006–0.0007 a.u & 1.162–1.221 a.u in pGr-5caC respectively. The small ρ(r), positive H(r), and –G(r)/V(r)≥1 values are clearly revealed that the π-π stacking interaction is occurred during complex formation in pGr-MBs complex. In B-pGr-5hmc complex, the calculated ρ(r) values of O_{62}–B_9 and N_{65}–B_{23} are 0.079 a.u and 0.114 a.u in B-pGr-5hmc. Similarly, in B-pGr-5fc and B-pGr-5caC complexes, the ρ(r) values of O_{61}–B_9 and O_{62}–B_{23} are 0.097 a.u and 0.109 a.u respectively. The higher ρ(r) values reveal that the covalent bond interactions occur between B-pGr and MBs which is to the presence of high electronegative atom (O/N) covalently interact with electropositive B atom, thus the reason B-pGr-MBs has higher adsorption energy (Berski et al., 2011). Further, the negative H(r) value and less than 1 (-G(r)/V(r)) values are also obtained in the B-pGr-MBs complex system which is indicating the existence of covalent interaction between B-pGr and MBs in a complex system. In N-pGr-MBs complexes, hydrogen bond interactions (N_{23}–H_{50}···O_{62} in N-pGr-5hmc, N_9–H_{39}···O_{61} in N-pGr-5fc, and N_{23}–H_{50}···N_{68} in N-pGr-5caC) occur between N-pGr and MBs. The calculated ρ(r) and $\nabla^2\rho$(r) values of hydrogen bonds are 0.030 a.u & 0.106 a.u (N_{23}–H_{50}···O_{62}), 0.023 a.u & 0.074 a.u (N_9–H_{39}···O_{61}), and 0.020 a.u & 0.062 a.u (N_{23}–H_{50}···N_{68}). The corresponding –G(r)/V(r) is 0.991 a.u (N_{23}–H_{50}···O_{62}), 0.969 a.u (N_9–H_{39}···O_{61}), and 0.943 a.u (N_{23}–H_{50}···N_{68}). The calculated AIM parameters illustrate that the covalent interaction occurs in B-pGr-MBs and non-covalent interaction occurs in pGr-MBs and N-pGr-MBs system.

The reduced density gradient (RDG) (Johnson et al., 2010) is calculated for MBs over p-GDs which is governing (physisorption/chemisorption) the interaction between MBs and p-GDs. The NCI map for a complex system is given in the Supplementary Fig. S1. In Fig. S1, ≈-0.050 to 0.050 a.u, −0.010 to −0.050 a.u, 0.010 to 0.050 a.u range indicates that van der Waals, hydrogen bond interaction, and steric effect respectively. In MBs on PGr complex, there is no hydrogen bond peaks are observed at −0.010 to −0.050 a.u region which shows that $\pi - \pi$ stacking interaction occurs during complex formation. In MBs on B-pGr complex, one peak is monitored at −0.020 a.u in 5hmc/5fc-B-pGr, whereas two peaks are observed at −0.020 and −0.030 a.u in 5 aC-B-pGr which is mainly due to the strong interaction occurred between B and N/O during complex formation. In the case of MBs on N-pGr, one peak is obtained at −0.030 a.u in 5 hmc-N-pGr, whereas in both 5fc-N-pGr and 5caC-N-pGr, one major peak is calculated at −0.025 a.u. These results show that the hydrogen bond interaction (N_{23}–H_{50}···O_{62} in N-pGr-5hmc, N_9–H_{39}···O_{61} in N-pGr-5fc, and N_{23}–H_{50}···N_{68} in N-pGr-5caC) has appeared between MBs and N-pGr.

3.6. Absorption spectra

The absorption properties of isolated MBs and MBs on p-GDs are reconnoitred by the TD-DFT method which is given in Fig. 6 and Table 7.

Previous experimental results (Chowdhury et al., 2014; Evertsz et al., 1994) have reported that the modified DNA absorption peak has occurred at 220–280 nm. In this investigation, isolated MBs such as 5hmc, 5fc, and 5caC maximum peaks are calculated at 205.1 nm, 244.9 nm, and 229.9 nm respectively, all these peaks are found to n-π* transition, these results are good agreement with previous results (Mato et al., 2017; Xing et al., 2018) and their corresponding orbital transition is H→L+2 (in 5hmc), H→L (in 5fc), and H→L+1 (in 5caC) respectively. Ai, Y et al. (Ai et al., 2018) reported that the excitation energy and oscillator strength of 5hmc were found at 4.789 eV and 0.035 respectively. In this work, the calculated excitation energy and oscillator strength values are 4.797 eV & 0.030 (in 5hmc), 5.062 eV & 0.384 (in 5fc), and 5.392 eV & 0.429 (in 5caC) respectively. These results are good agreement with the previous result (Ai et al., 2018; Mato et al., 2017). When MBs over the p-GDs, the maximum peaks are shifted towards higher wavelength which exhibits bathochromic shift. In MBs-pGr complex system, the calculated maximum adsorption peak and excitation energy are 244.6 nm & 5.067 eV (in pGr-5hmc), 250.7 nm & 4.945 eV (in pGr-5fc), and 249.3 nm & 4.972 eV (in pGr-5caC). The calculated corresponding oscillator strength of MBs-pGr complex are 0.429, 0.041, and 0.022, their corresponding orbital transition arises at H-2→L, H→L, and H-2→L, it exhibits hypochromic effect. In B-pGr-MBs complex, the maximum absorption peak is observed at 469.8 nm, 542.1 nm, and 503.3 nm. Compared with pGr-MBs, B-pGr-MBs has a higher wavelength which is mainly due to the presence of B dopant atoms in the porous region. The B dopant atoms decrease the energy gap between HOMO and LUMO and it is adsorbed more MBs than the pGr. Increasing wavelength decreases the excitation energy (Saravanan et al, 2020a, 2020b; Vinnarasi et al., 2019), the calculated excitation energy values of MBs-B-pGr complexes are 2.639 eV (in B-pGr-5hmc), 2.287 eV (in

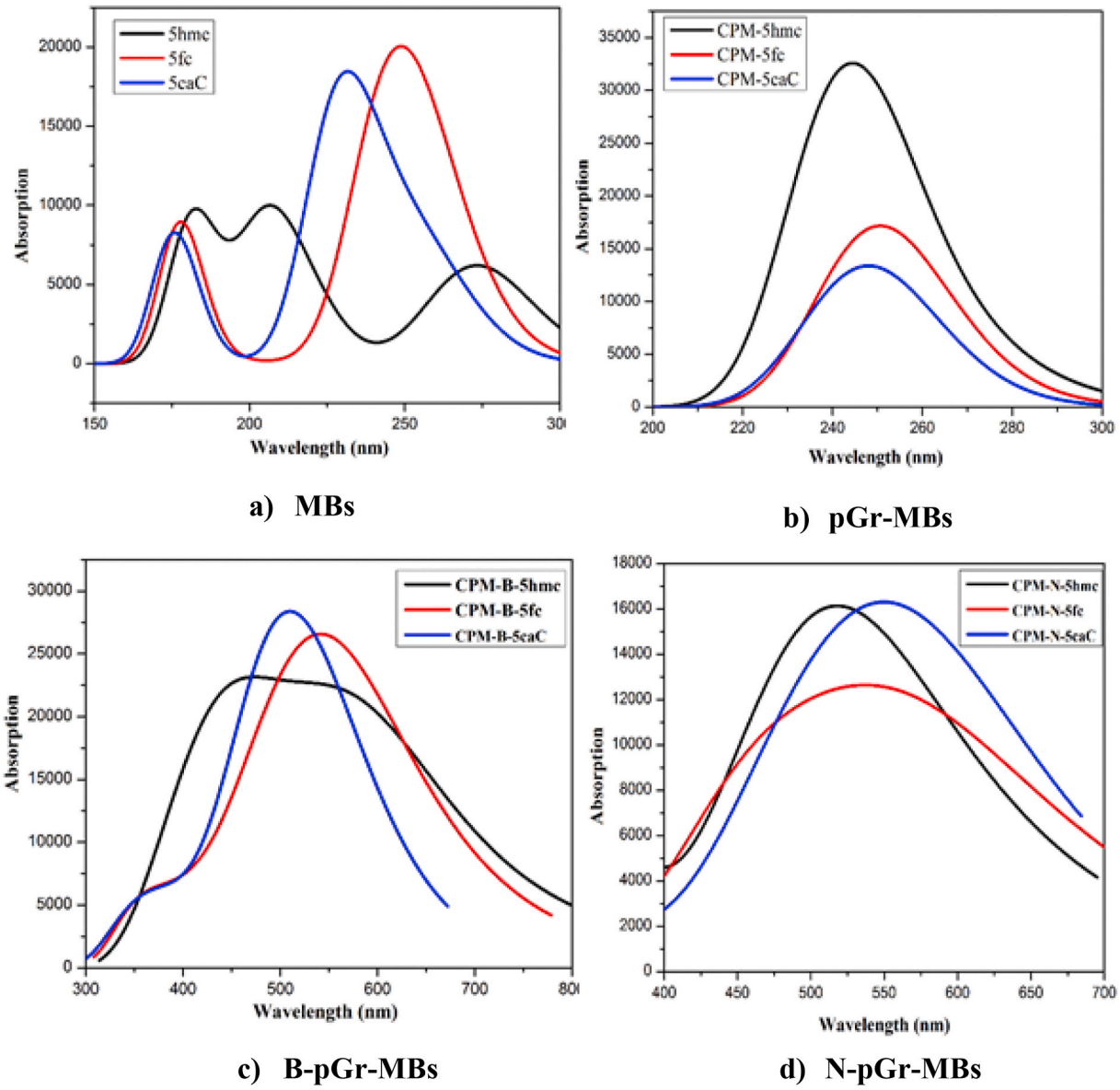

Fig. 6. Absorption spectra of isolated and their complex structures.

B-pGr-5fc), and 2.406 eV (in pGr-5caC) respectively. The corresponding orbital transitions of B-pGr-MBs complexes are H-1→ L+1, H-1→ L, and H-1→L. Whereas, in the case of MBs-N-pGr, the absorption peaks are also shifted to a higher wavelength. The maximum peaks are obtained at 523.8 nm (in N-pGr-5hmc), 565.3 nm (in N-pGr-5fc), and 561.0 nm (in N-pGr-5caC) respectively, which exhibits bathochromic shift. The obtained results strongly expose that the presence B and N dopant atoms reduces the energy gap and increase the chemical reactivity, thus they are adsorbed more MBs than the pGr. The present investigation strongly reported that the B-pGr would be expedient in the optical sensing of epigenetically modified nucleobases.

4. Conclusion

In the present investigation, pGr, B-pGr, and N-pGr are explored as a sensing device of epigenetically modified DNA bases by the quantum chemical method based on DFT theory. The structural and electronic properties reveal that B-pGr is more reactive than the pGr and N-pGr, due to the empty p-orbitals of B atom which easily interact with partially filled occupied p-orbital of N and O atom. Thus, the MBs on B-pGr have high adsorption energy than the other complexes, because two covalent bonds (O_{62}–B_9 & N_{65}–B_{23}) interactions occur between B-pGr and 5hmc during complex formation. The obtained results are compared with previous results. The adsorption energy of B-pGr-MBs are −96.074 kcal/mol (in B-pGr-5hmc), −60.721 kcal/mol (in B-pGr-5fc), and −77.0 kcal/mol (in B-pGr-5caC). The positive ΔN values (0.005 eV, 0.076 eV, and 0.047 in MBs on pGr and 0.171 eV, 0.252 eV and 0.205 eV in MBs on N-pGr) show that the charge is transferred from pGr and N-pGr to MBs, the negative ΔN values (−0.141 eV, −0.032 eV, and −0.061 eV in MBs on B-pGr) indicate the charge is transferred from MBs to B-pGr. Further, it is confirmed by NBO and EDDM analysis. The effect of absorption properties shows that the B-pGr is strongly adsorbed MBs at 342 nm. The obtained results exhibit that the B-pGr is an optimal choice for sensing device of epigenetically modified DNA bases in cancer therapy.

Authorship statements

Vinnarasi Saravanan: Roles/Writing - original draft. Akilan Rajamani: Software; Validation; Visualization. Shankar Ramasamy: Supervision, Formal analysis. Alaa Baazeem: Formal analysis. Indra Raj

Table 7
The absorption spectra of isolated and complex structures are calculated by TD-DFT.

Complex	Wavelength (nm)	Excitation energy (eV)	Oscillator strength	Orbital transition
5 hmc	205.1	4.797 (4.77)*[a]	0.030	H→L+2
5fc	244.9	5.061 (4.56)*[a]	0.384	H→L
5caC	229.9	5.392	0.429	H→L+1
pGr-5hmc	244.6	5.067	0.012	H-2→L
B-pGr-5hmc	469.8	2.639	0.288	H-1→L+1
N-pGr-5hmc	523.8	2.366	0.109	H-2→L
pGr-5fc	250.7	4.945	0.041	H→L
B-pGr-5fc	542.1	2.287	0.319	H-1→L
N- pGr-5fc	565.3	2.193	0.128	H→L+4
pGr-5caC	249.3	4.972	0.022	H-2→L
B-pGr-5caC	503.3	2.406	2.463	H-1→L
N-pGr-5caC	561.0	2.209	0.076	H→L+2

*[a] Ref (Mato et al., 2017).

Upadhyaya c- Formal analysis

Declaration of competing interest

The authors declare that they have no known competing financial interests or personal relationships that could have appeared to influence the work reported in this paper.

Acknowledgements

The author Dr. Shankar Ramasamy acknowledges the financial support from Rashtriya Uchchatar Shiksha Abhiyan (RUSA), India (Official Memorandum no. IQAC/RUSA2.0/PA/2021/1 dated January 08, 2021). The authors extend their appreciation to Taif University for funding current work by Taif University Researchers Supporting Project number (TURSP-2020/295), Taif University, Taif, Saudi Arabia.

Appendix A. Supplementary data

Supplementary data to this article can be found online at https://doi.org/10.1016/j.envres.2021.111133.

References

Agnoli, S., Favaro, M., 2016. Doping graphene with boron: a review of synthesis methods, physicochemical characterization, and emerging applications. J. Mater. Chem. 4, 5002–5025. https://doi.org/10.1039/c5ta10599d.

Ai, Y., Xing, J., Zhang, A., Zhao, C., Liu, Y., Xie, B., Chen, W., Cui, G., Lu, Z., Wang, X., 2018. Computational study on the excited-state decay of 5-methylcytosine and 5-hydroxymethylcytosine: the common form of DNA methylation and its oxidation product. J. Phys. Chem. B 122, 10424–10434. https://doi.org/10.1021/acs.jpcb.8b07830.

AlZahrani, A.Z., Srivastava, G.P., 2010. Structural and electronic properties of H-passivated graphene. Appl. Surf. Sci. 256, 5783–5788. https://doi.org/10.1016/j.apsusc.2010.03.088.

Andriotis, A.N., Richter, E., Menon, M., 2016. Prediction of a new graphenelike Si2BN solid. Phys. Rev. B 93, 2–4. https://doi.org/10.1103/PhysRevB.93.081413.

Ao, Z.M., Li, S., Jiang, Q., 2010. Correlation of the applied electrical field and CO adsorption/desorption behavior on Al-doped graphene. Solid State Commun. 150, 680–683. https://doi.org/10.1016/j.ssc.2009.12.016.

Bader, R.F.W., 1991a. A quantum theory of molecular structure and its applications. Chem. Rev. 91, 893–928. https://doi.org/10.1021/cr00005a013.

Bader, R.F.W., 1991b. A quantum theory of molecular structure and its applications. Chem. Rev. 91, 893–928. https://doi.org/10.1021/cr00005a013.

Bader, R.F.W., 1998. A bond path: a universal indicator of bonded interactions. J. Phys. Chem. 102, 7314–7323. https://doi.org/10.1021/jp981794v.

Berski, S., Latajka, Z., Gordon, A.J., 2011. On the multiple B–N bonding in boron compounds using the topological analysis of electron localization function (ELF). New J. Inside Chem. 35, 89–96. https://doi.org/10.1039/C0NJ00517G.

Bian, K., Lenz, S.A.P., Tang, Q., Chen, F., Qi, R., Jost, M., Drennan, C.L., Essigmann, J.M., Wetmore, S.D., Li, D., 2019. DNA repair enzymes ALKBH2, ALKBH3, and AlkB oxidize 5-methylcytosine to 5-hydroxymethylcytosine, 5-formylcytosine and 5-carboxylcytosine in vitro. Nucleic Acids Res. 47, 5522–5529. https://doi.org/10.1093/nar/gkz395.

Chai, J.-D., Head-Gordon, M., 2008. Systematic optimization of long-range corrected hybrid density functionals. J. Chem. Phys. 128 https://doi.org/10.1063/1.2834918, 084106.

Cheng, Y., Bernstein, A., Chen, D., Jin, P., 2015. 5-Hydroxymethylcytosine: a new player in brain disorders? Exp. Neurol. 268, 3–9. https://doi.org/10.1016/j.expneurol.2014.05.008.

Chowdhury, B., Cho, I.-H., Hahn, N., Irudayaraj, J., 2014. Quantification of 5-methylcytosine, 5-hydroxymethylcytosine and 5-carboxylcytosine from the blood of cancer patients by an enzyme-based immunoassay. Anal. Chim. Acta 852, 212–217. https://doi.org/10.1016/j.aca.2014.09.020.

Dai, J., Yuan, J., Giannozzi, P., 2009. Gas adsorption on graphene doped with B, N, Al, and S: a theoretical study. Appl. Phys. Lett. 95, 232105 https://doi.org/10.1063/1.3272008.

Dolinoy, D., Weidman, J., Jirtle, R., 2007. Epigenetic gene regulation: linking early developmental environment to adult disease. Reprod. Toxicol. 23, 297–307. https://doi.org/10.1016/j.reprotox.2006.08.012.

Evertsz, E.M., Rippe, K., Jovin, T.M., 1994. Parallel-stranded duplex DNA containing blocks of trans purine-purine and purine-pyrimidine base pairs. Nucleic Acids Res. 22, 3293–3303. https://doi.org/10.1093/nar/22.16.3293.

Frisch, M.J., Trucks, G.W., Schlegel, H.B., Scuseria, G.E., Robb, M.A., Cheeseman, J.R., Scalmani, G., Barone, V., Mennucci, B., Petersson, G.A., Nakatsuji, H., Caricato, M., Li, X., Hratchian, H.P., Izmaylov, A.F., Bloino, J., Zheng, G., Sonnenberg, J.L., 2009. J.C. and D.J.F. Gaussian 09.

Gao, H., Feng, W., Li, X., Li, N., Du, Y., Wu, Y., Bai, H., Qiao, W., 2019. Insights into the non-covalent interaction between modified nucleobases and graphene nanoflake from first-principles. Phys. E Low-dimensional Syst. Nanostructures 107, 73–79. https://doi.org/10.1016/j.physe.2018.11.002.

Gershow, M., Golovchenko, J.A., 2007. Recapturing and trapping single molecules with a solid-state nanopore. Nat. Nanotechnol. 2, 775–779. https://doi.org/10.1038/nnano.2007.381.

Hahn, M.A., Szabó, P.E., Pfeifer, G.P., 2014. 5-Hydroxymethylcytosine: a stable or transient DNA modification? Genomics 104, 314–323. https://doi.org/10.1016/j.ygeno.2014.08.015.

Hatchwell, E., Greally, J.M., 2007. The potential role of epigenomic dysregulation in complex human disease. Trends Genet. 23, 588–595. https://doi.org/10.1016/j.tig.2007.08.010.

He, Y.-F., Li, B.-Z., Li, Z., Liu, P., Wang, Y., Tang, Q., Ding, J., Jia, Y., Chen, Z., Li, L., Sun, Y., Li, X., Dai, Q., Song, C.-X., Zhang, K., He, C., Xu, G.-L., 2011. Tet-mediated formation of 5-carboxylcytosine and its excision by TDG in mammalian DNA. Science 333, 1303–1307. https://doi.org/10.1126/science.1210944.

Hu, S., Yong, Y., Li, C., Zhao, Z., Jia, H., Kuang, Y., 2020. The Si2BN monolayers as promising candidates for hydrogen storage. Phys. Chem. Chem. Phys. https://doi.org/10.1039/D0CP00943A.

Ito, S., Shen, L., Dai, Q., Wu, S.C., Collins, L.B., Swenberg, J.A., He, C., Zhang, Y., 2011. Tet proteins can convert 5-methylcytosine to 5-formylcytosine and 5-carboxylcytosine. Science 333 (80), 1300–1303. https://doi.org/10.1126/science.1210597.

Johnson, E.R., Keinan, S., Mori-Sánchez, P., Contreras-García, J., Cohen, A.J., Yang, W., 2010. Revealing noncovalent interactions. J. Am. Chem. Soc. 132, 6498–6506. https://doi.org/10.1021/ja100936w.

Kamel, M., Raissi, H., Morsali, A., 2017. Theoretical study of solvent and co-solvent effects on the interaction of Flutamide anticancer drug with Carbon nanotube as a drug delivery system. J. Mol. Liq. 248, 490–500. https://doi.org/10.1016/j.molliq.2017.10.078.

Kasianowicz, J.J., Brandin, E., Branton, D., Deamer, D.W., 1996. Characterization of individual polynucleotide molecules using a membrane channel. Proc. Natl. Acad. Sci. Unit. States Am. 93, 13770–13773. https://doi.org/10.1073/pnas.93.24.13770.

Kong, X., Sun, Z., Chen, Q., 2012. The positive influence of boron-doped graphene for its supported Au clusters: enhancement of SERS and oxygen molecule adsorption. Phys. Chem. Chem. Phys. 14, 13564 https://doi.org/10.1039/c2cp42297b.

Langreth, D.C., Dion, M., Rydberg, H., Schröder, E., Hyldgaard, P., Lundqvist, B.I., 2005. Van der Waals density functional theory with applications. Int. J. Quant. Chem. 101, 599–610. https://doi.org/10.1002/qua.20315.

Li, S., Yang, Z.-D., Zhang, G., Zeng, X.C., 2015. Electronic and transport properties of porous graphene sheets and nanoribbons: benzo-CMPs and BN codoped derivatives. J. Mater. Chem. C 3, 9637–9649. https://doi.org/10.1039/C5TC01954K.

Liu, J., Cui, L., Losic, D., 2013. Graphene and graphene oxide as new nanocarriers for drug delivery applications. Acta Biomater. 9, 9243–9257. https://doi.org/10.1016/j.actbio.2013.08.016.

Louit, G., Hocquet, A., Ghomi, M., Meyer, M., Sühnel, J., 2003. Guanine tetrads interacting with metal ions. An AIM topological analysis of the electronic density. PhysChemComm 6, 1–5. https://doi.org/10.1039/b210911e.

Lu, T., Chen, F., 2012. Multiwfn: a multifunctional wavefunction analyzer. J. Comput. Chem. 33, 580–592. https://doi.org/10.1002/jcc.22885.

Lu, X., Zhao, B.S., He, C., 2015. TET family proteins: oxidation activity, interacting molecules, and functions in diseases. Chem. Rev. 115, 2225–2239. https://doi.org/10.1021/cr500470n.

Matito, E., Salvador, P., Duran, M., Solà, M., 2006. Aromaticity measures from fuzzy-atom bond orders (FBO). The aromatic fluctuation (FLU) and the para-delocalization (PDI) indexes. J. Phys. Chem. 110, 5108–5113. https://doi.org/10.1021/jp057387i.

Mato, J., Keipert, K., Gordon, M.S., 2017. Excited state properties of 5-formylcytosine and 5-hydroxymethylcytosine. Mol. Phys. 115, 2721–2730. https://doi.org/10.1080/00268976.2017.1311424.

Meng, S., Zhou, H., Feng, Z., Xu, Z., Tang, Y., Wu, M., 2019. Epigenetics in neurodevelopment: emerging role of circular RNA. Front. Cell. Neurosci. 13 https://doi.org/10.3389/fncel.2019.00327.

Mudedla, S.K., Balamurugan, K., Subramanian, V., 2014. Computational study on the interaction of modified nucleobases with graphene and doped graphenes. J. Phys. Chem. C 118, 16165–16174. https://doi.org/10.1021/jp503126q.

Mudedla, S.K., Balamurugan, K., Kamaraj, M., Subramanian, V., 2016. Interaction of nucleobases with silicon doped and defective silicon doped graphene and optical properties. Phys. Chem. Chem. Phys. 18, 295–309. https://doi.org/10.1039/c5cp06059a.

Parthasarathi, R., Subramanian, V., Sathyamurthy, N., 2006. Hydrogen bonding without borders: an atoms-in-molecules perspective. J. Phys. Chem. 110, 3349–3351. https://doi.org/10.1021/jp060571z.

Pashangpour, M., Ghaffari, V., 2013. Investigation of structural and electronic transport properties of graphene and graphane using maximally localized Wannier functions. J. Theor. Appl. Phys. 7 (9) https://doi.org/10.1186/2251-7235-7-9.

Petronis, A., 2010. Epigenetics as a unifying principle in the aetiology of complex traits and diseases. Nature 465, 721–727. https://doi.org/10.1038/nature09230.

Portela, A., Esteller, M., 2010. Epigenetic modifications and human disease. Nat. Biotechnol. 28, 1057–1068. https://doi.org/10.1038/nbt.1685.

Reed, A.E., Curtiss, L.A., Weinhold, F., 1988. Intermolecular interactions from a natural bond orbital. Donor—Acceptor Viewpoint. Chem. Rev. 88, 899–926. https://doi.org/10.1021/cr00088a005.

Saha, B., Bhattacharyya, P.K., 2016. Understanding reactivity, aromaticity and absorption spectra of carbon cluster mimic to graphene: a DFT study. RSC Adv. 6, 79768–79780. https://doi.org/10.1039/C6RA15016K.

Salzner, U., Aydin, A., 2011. Improved prediction of properties of π-conjugated oligomers with range-separated hybrid density functionals. J. Chem. Theor. Comput. 7, 2568–2583. https://doi.org/10.1021/ct2003447.

Saravanan, V., Rajamani, A., Subramani, M., Ramasamy, S., 2020a. Exploring two-dimensional graphene and boron-nitride as potential nanocarriers for cytarabine and clofarabine anti-cancer drugs. Comput. Biol. Chem. 107334 https://doi.org/10.1016/j.compbiolchem.2020.107334.

Saravanan, V., Rajamani, A., Vasudevan, S., Ramasamy, S., 2020b. Exploring the nature of interaction and stability between DNA/RNA base pairs and defective & defect-dopant graphene sheets. A possible insights on DNA/RNA sequencing. Int. J. Biol. Macromol 146, 387–404. https://doi.org/10.1016/j.ijbiomac.2020.01.001.

Saravanan, V., Rajamani, A., Vasudevan, S., Ramasamy, S., 2020c. Exploring the nature of interaction and stability between DNA/RNA base pairs and defective & defect-dopant graphene sheets. A possible insights on DNA/RNA sequencing. Int. J. Biol. Macromol 146, 387–404. https://doi.org/10.1016/j.ijbiomac.2020.01.001.

Schübeler, D., 2015. Function and information content of DNA methylation. Nature 517, 321–326. https://doi.org/10.1038/nature14192.

Shukla, V., Araujo, R.B., Jena, N.K., Ahuja, R., 2017. The curious case of two dimensional Si2BN: a high-capacity battery anode material. Nanomater. Energy 41, 251–260. https://doi.org/10.1016/j.nanoen.2017.09.026.

Singh, D., Gupta, S.K., Sonvane, Y., Ahuja, R., 2017. High performance material for hydrogen storage: graphenelike Si2BN solid. Int. J. Hydrogen Energy. https://doi.org/10.1016/j.ijhydene.2017.07.082, 42, 22942.

Sofo, J.O., Chaudhari, A.S., Barber, G.D., 2007. Graphane: a two-dimensional hydrocarbon. Phys. Rev. B - Condens. Matter Mater. Phys. 75, 1–4. https://doi.org/10.1103/PhysRevB.75.153401.

Szwagierczak, A., Bultmann, S., Schmidt, C.S., Spada, F., Leonhardt, H., 2010. Sensitive enzymatic quantification of 5-hydroxymethylcytosine in genomic DNA. Nucleic Acids Res. 38 https://doi.org/10.1093/nar/gkq684 e181–e181.

Tabatabaei, S.-M., Pourfath, M., Fathipour, M., 2018. Adsorption characteristics of epigenetically modified DNA nucleobases on single-layer MoS 2 : a first-principles study. J. Appl. Phys. 124, 134501 https://doi.org/10.1063/1.5034004.

Taylor, P., Boys, S.F., Bernardi, F., 1970. Boys. n.d. https://doi.org/10.1080/00268977000101561, 37, 41.

Vatanparast, M., Shariatinia, Z., 2018. Computational studies on the doped graphene quantum dots as potential carriers in drug delivery systems for isoniazid drug. Struct. Chem. 29, 1427–1448. https://doi.org/10.1007/s11224-018-1129-x.

Vinnarasi, S., Radhika, R., Vijayakumar, S., Shankar, R., 2019. Structural insights into the anti-cancer activity of quercetin on G-tetrad, mixed G-tetrad, and G-quadruplex DNA using quantum chemical and molecular dynamics simulations. J. Biomol. Struct. Dyn. 1–23. https://doi.org/10.1080/07391102.2019.1574239, 0.

Wang, J., Chen, Y., Yuan, L., Zhang, M., Zhang, C., 2019. Scandium decoration of boron doped porous graphene for high-capacity hydrogen storage. Molecules 24 (2382). https://doi.org/10.3390/molecules24132382.

Wasalathilake, K.C., Ayoko, G., n.d. Porous graphene materials for energy storage and conversion applications 1–19.

Xing, J., Ai, Y., Liu, Y., Du, J., Chen, W., Lu, Z., Wang, X., 2018. Theoretical studies on the photophysics and photochemistry of 5-formylcytosine and 5-carboxylcytosine: the oxidative products of epigenetic modification of cytosine in DNA. J. Phys. Chem. B 122, 2704–2714. https://doi.org/10.1021/acs.jpcb.7b10218.

Xu, P., Yang, J., Wang, K., Zhou, Z., Shen, P., 2012. Porous graphene: properties, preparation, and potential applications. Chin. Sci. Bull. 57, 2948–2955. https://doi.org/10.1007/s11434-012-5121-3.

Xu, L., Chen, Y.-C., Nakajima, S., Chong, J., Wang, L., Lan, L., Zhang, C., Wang, D., 2014. A chemical probe targets DNA 5-formylcytosine sites and inhibits TDG excision, polymerases bypass, and gene expression. Chem. Sci. 5, 567–574. https://doi.org/10.1039/C3SC51849C.

Zhang, X., Xin, J., Ding, F., 2013. The edges of graphene. Nanoscale 5 (2556). https://doi.org/10.1039/c3nr34009k.

Zhao, Y., Truhlar, D.G., 2008. The M06 suite of density functionals for main group thermochemistry, thermochemical kinetics, noncovalent interactions, excited states, and transition elements: two new functionals and systematic testing of four M06-class functionals and 12 other function. Theor. Chem. Acc 120, 215–241. https://doi.org/10.1007/s00214-007-0310-x.